

X-RAYS FROM CEPHEUS A EAST AND WEST

STEVEN H. PRAVDO

Jet Propulsion Laboratory, California Institute of Technology, 306-431, 4800 Oak Grove Drive,
Pasadena, CA 91109; spravdo@jpl.nasa.gov

AND

YOHKO TSUBOI

Department of Physics, Faculty of Science and Engineering, Chuo University, Kasuga 1-13-27, Bunkyo-ku,
Tokyo 112-8551, Japan; tsuboi@phys.chuo-u.ac.jp

Received 2004 December 22; accepted 2005 February 25

ABSTRACT

We report the discovery of X-rays from both components of Cepheus A, East and West, with the *XMM-Newton* observatory. HH 168 joins the ranks of other energetic Herbig-Haro objects that are sources of $T \geq 10^6$ K X-ray emission. The effective temperature of HH 168 is $T = 5.8_{-2.3}^{+3.5} \times 10^6$ K, and its unabsorbed luminosity is 1.1×10^{29} ergs s^{-1} , making it hotter and less luminous than other representatives of its class. We also detect prominent X-ray emission from the complex of compact radio sources believed to be the power sources for Cep A. We call this source HWX, and it is distinguished by its hard X-ray spectrum, $T = 1.2_{-0.5}^{+1.2} \times 10^8$ K, and its complex spatial distribution. It may arise from one or more protostars associated with the radio complex, the outflows, or a combination of the two. We detect 102 X-ray sources, many presumed to be pre-main-sequence stars on the basis of the reddening of their optical and IR counterparts.

Subject headings: ISM: Herbig-Haro objects — X-rays: ISM

1. INTRODUCTION

Cep A is a star formation region (Sargent 1977) at a distance of ~ 730 pc (Johnson 1957). It consists of two main H II regions, Cep A East and Cep A West (Hughes & Wouterloot 1982). The eastern region is resolved into several compact radio sources (Hughes & Wouterloot 1984), radio jets (Rodríguez et al. 1994), and masers (Blitz & Lada 1979). The western region also contains compact radio sources (Hughes & Moriarty-Schieven 1990) and Herbig-Haro (HH) object 168 (GGD 37; Gyulbudaghian et al. 1978). The latter shows the characteristics of other energetic HH optical condensations with high excitation and line widths (Hartigan et al. 1986) and high velocities and proper motions (Lenzen 1988). Hartigan & Lada (1985) identified several optical knots within HH 168 that were resolved and further analyzed with *Hubble Space Telescope* (*HST*) spectroscopy (Hartigan et al. 2000).

An enduring question is the identification of the power source or sources in this active region. Much of the attention has focused on two compact radio sources, HW 2 and HW 3d (Rodríguez et al. 1980; Hughes & Wouterloot 1984). Torrelles et al. (1985) estimate that each source harbors a zero-age main-sequence B1 star to account for the $\sim 2 \times 10^4 L_{\odot}$ in infrared luminosity (Beichman et al. 1979). Polarization results point toward HW 2 as the power source (Casement & McLean 1996). However, whether these objects power HH 168 (Lenzen et al. 1984) is a matter of contention. Lenzen (1988) measured the proper motions for six of the HH 168 knots and concluded that the vectors are directed away from HW 2 and HW 3, “localizing the center of acceleration near this position.” Alternatively, Garay et al. (1996) suggest that an ultracompact, variable radio source within the HH 168 HW knot powers the other knots in their east-to-west motion. In this paper we weigh in with the X-ray evidence.

2. OBSERVATIONS AND ANALYSIS

2.1. X-Ray Sources

We observed Cep A with the EPIC cameras of the *XMM-Newton* observatory on 2003 August 23 for 43.9 ks. The

cameras were in the standard imaging mode. We analyzed the data using the *XMM-Newton* Science Analysis System (SAS)¹ and other standard software packages discussed below. EPIC is composed of three cameras: pn, MOS1, and MOS2. We filtered the raw event data using canonical energy, event type, and high count rate criteria. This resulted in net observing times of 37.5 ks for pn and 43.1 ks for MOS1 and MOS2. The results of all cameras are consistent. We display spectral data using the pn camera because it has a higher count rate and spatial data using the MOS cameras because their smaller pixel size, $1''.1$ versus $4''.1$, allows better sampling.

We performed source detection on all the data in two energy bands: 0.2–1 keV (“soft”) and 1–10 keV (“hard”). A mosaic image of the filtered data from all three cameras is shown in Figure 1 with the detected sources superposed. The 24 soft sources are shown with red squares, and the 85 hard sources are shown with blue circles. The spot size diameter for a point source viewed with the *XMM-Newton* telescope and camera is about $5''$. We therefore use this diameter for the source symbols in Figure 1. Seven of the sources appear in both bands, where the criterion for a match between the bands is a positional offset of $< 2''.5$. The average and standard deviations of the offsets between the hard and soft source matches are R.A. = $-0''.2 \pm 0''.3$ and decl. = $-0''.2 \pm 1''.0$. Thus, the total number of distinct X-ray sources detected is 102.

We compared the 102 X-ray sources with the USNO-B1.0 (Monet et al. 2003) and Two Micron All Sky Survey (2MASS) catalogs. The statistical results are shown in Table 1, where the criterion for a match between the X-ray source and the catalog source is again a positional offset of $< 2''.5$. Table 2 lists the sources, their X-ray properties, and their optical and infrared magnitudes. Figure 2 shows the *JHK* color-color diagram for the 62 sources detected. The solid curve at the bottom left is the

¹ SAS Users’ Guide available at http://xmm.vilspa.esa.es/external/xmm_user_support/documentation/sas_usg/USG/node1.html.

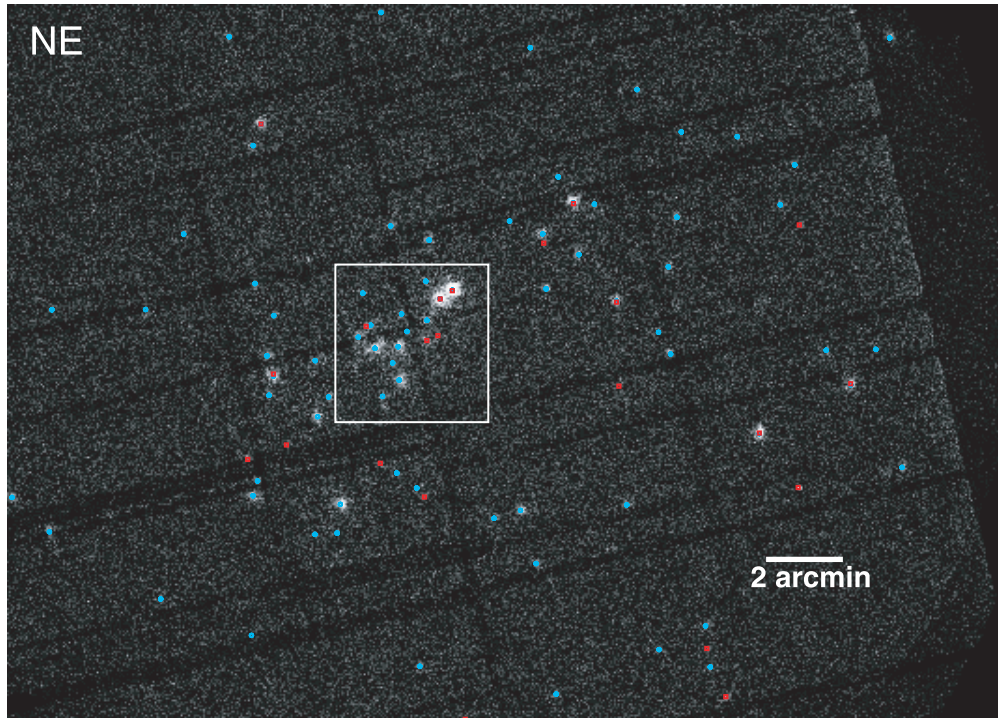


FIG. 1.— Composite X-ray image of Cep A from three *XMM-Newton* cameras. Red squares mark the locations of soft X-ray sources (0.2–1.0 keV), while blue circles mark the locations of hard X-ray sources (1.0–10.0 keV). The box shows the portion of the image enlarged in Fig. 3.

main sequence, while the dashed curves show the lines of reddening. The majority of the objects fall along these reddening curves in the locations of pre-main-sequence stars (PMSs), including weak-line T Tauri stars and classical T Tauri stars. The source XMMPT J225454.9+615936 (see below) falls in the main-sequence region. A number of outlying sources are labeled and discussed below.

Thirty-nine sources have neither optical nor IR counterparts. Most of these, 29, are detected in the hard band only, and 10 are detected in the soft band only.

2.2. HH 168

The source detection algorithm found two soft X-ray sources within HH 168. Figure 3 (*left*) shows the soft-band image. Note that the sources are predominantly soft X-ray sources, as they are not apparent in the harder X-ray image (Fig. 3, *right*). The two sources XMMPT J225607.1+620159 and XMMPT J225604.7+620207 are labeled X1 and X2, respectively. Figure 4 shows an $H\alpha$ image of the region taken with the *HST* WFPC2. We have superposed X-ray contours and the locations of the soft X-ray sources (*squares*) on the image. The prominent HH knots S, D, E, and HW (Hartigan & Lada 1985) are also labeled. The X-ray emission is highest at the southeastern source, XMMPT J225607.1+

620159, which is detected with a statistical significance of 4σ in each of the three cameras and a net of 91 counts. The northwestern source, XMMPT J225604.7+620207, is detected at 4, 2, and 3σ in the pn, MOS1, and MOS2 cameras, respectively, with a net of 58 counts. There is no evidence for intensity variability in these sources.

The peaks of the X-ray emission within HH 168 are significantly offset by several arcseconds from the brightest $H\alpha$ knots. They are located on the edges of knots E and D. Another smaller enhancement is located near knot HW. The X-ray contours in Figure 4 suggest that these two sources are part of a larger extended emission that covers the entire region of enhanced $H\alpha$ emission. We compared the radial profiles at the same energies of the soft X-ray emission with that of an expected neutron star point source, RX J171012.3–28075 (Y. Maeda 2004, private communication), and find that the data are consistent with extended emission (Fig. 5, *left*). We treated the emission as extended and extracted events from a circular region ($18''$ radius) containing both sources to perform spectroscopy with the XSPEC program. There were 150 net counts using either of two chosen background regions east and west of the sources. We fitted the spectrum with models containing interstellar absorption (e.g., WABS) and continuum emission, either thin thermal bremsstrahlung (e.g., MEKA-L)

TABLE 1
OPTICAL AND INFRARED MATCHES FOR Cep A X-RAY SOURCES

X-Ray Sources	Catalog	Number of Matches	R.A. Offset (arcsec)	Decl. Offset (arcsec)
Soft band (0.2–1 keV)	USNO-B1.0	12	-0.3 ± 1.1	-0.6 ± 0.8
	2MASS	12	-0.3 ± 1.0	-0.5 ± 1.0
Hard band (1–10 keV)	USNO-B1.0	39	-0.04 ± 1.0	-0.01 ± 1.0
	2MASS	56	-0.1 ± 0.9	0.2 ± 1.0

TABLE 2
Cep A X-RAY SOURCES

XMMPT Source	R.A. (deg)	Decl. (deg)	σ	Soft (counts ks ⁻¹)	Hard (counts ks ⁻¹)	USNO-B1.0	<i>B</i>	<i>R</i>	<i>I</i>	2MASS	<i>J</i>	<i>H</i>	<i>K_s</i>	Notes
J225424.0+615843.....	343.5998	61.9788	7.0	...	2.95	22542385+6158458	13.242	12.104	11.604	
J225426.1+620941.....	343.6087	62.1614	10.9	...	5.16	
J225429.5+620144.....	343.6227	62.0291	4.3	...	1.39	
J225435.0+620050.....	343.6461	62.0141	14.0	0.97	7.57	1520-0380634	18.35	15.36	14.16	22543509+6200526	12.253	11.41	11.066	
J225440.3+620143.....	343.6676	62.0288	8.0	...	3.77	
J225446.0+620455.....	343.6919	62.0821	4.7	1.04	...	1520-0380668	20.56	18.44	16.62	22544615+6204568	14.871	14.277	13.979	
J225446.5+615813.....	343.6937	61.9705	8.1	2.21	
J225447.0+620627.....	343.6960	62.1077	7.2	...	2.85	1521-0407040	...	18.88	17.17	22544706+6206260	14.216	12.962	12.404	
J225450.1+620526.....	343.7094	62.0907	7.4	...	3.33	
J225454.9+615936.....	343.7294	61.9935	20.8	7.99	8.34	1519-0362104	15.25	13.46	12.40	22545508+6159382	11.753	11.239	11.04	RXH
J225459.5+620711.....	343.7478	62.1198	5.3	...	1.99	22545943+6207113	16.613	15.774	15.237	
J225501.6+621110.....	343.7573	62.1864	6.7	...	2.51	1521-0407079	...	19.34	16.96	22550178+6211114	14.543	13.311	12.841	
J225502.3+615254.....	343.7603	61.8817	6.7	1.84	...	1518-0358642	14.29	12.92	12.06	22550222+6152545	11.499	11.129	11.006	
J225505.7+615339.....	343.7740	61.8943	4.5	...	1.66	1518-0358658	...	19.03	17.08	22550561+6153399	14.713	13.732	13.293	
J225506.4+615408.....	343.7769	61.9022	5.8	1.59	
J225506.7+615442.....	343.7779	61.9119	6.1	...	2.58	1519-0362122	19.96	16.90	15.38	22550663+6154439	13.324	12.32	11.96	
J225511.7+620718.....	343.7992	62.1218	3.9	...	1.17	22551184+6207175	16.816	15.329	15.033	
J225512.7+620507.....	343.8034	62.0855	7.3	...	3.08	
J225514.1+620138.....	343.8094	62.0274	8.4	...	4.14	
J225514.6+620352.....	343.8114	62.0645	7.0	...	2.95	1520-0380748	19.90	17.20	15.99	22551470+6203504	14.122	13.089	12.765	
J225516.7+615406.....	343.8201	61.9018	5.6	...	2.08	22551690+6154076	15.788	14.834	14.308	
J225516.7+620211.....	343.8205	62.0366	5.0	...	1.74	
J225521.3+620823.....	343.8394	62.1399	6.1	...	2.28	
J225523.7+615748.....	343.8493	61.9633	9.2	...	4.32	1519-0362154	...	18.89	16.80	22552398+6157477	14.019	12.78	12.214	
J225525.4+620049.....	343.8562	62.0138	4.0	0.89	22552563+6200518	12.425	11.991	11.86	
J225525.9+620259.....	343.8583	62.0499	13.0	2.01	5.31	1520-0380776	18.49	15.51	14.23	22552603+6202593	12.791	11.902	11.644	
J225530.7+620527.....	343.8778	62.0911	7.6	...	3.57	22553077+6205276	9.843	9.404	9.142	
J225534.0+620410.....	343.8925	62.0697	12.3	...	7.00	1520-0380793	...	18.74	16.77	22553429+6204114	13.663	12.229	11.682	
J225535.2+620530.....	343.8970	62.0918	19.7	0.69	13.87	22553538+6205320	14.351	13.001	12.432	
J225538.6+620610.....	343.9109	62.1028	4.4	...	1.54	
J225539.1+615258.....	343.9135	61.8829	5.0	...	1.86	
J225541.2+620318.....	343.9216	62.0552	8.2	...	3.45	1520-0380801	20.26	19.14	16.52	22554138+6203195	14.353	13.065	12.548	
J225541.7+620428.....	343.9239	62.0746	3.9	0.77	
J225542.0+620442.....	343.9250	62.0786	11.1	...	6.35	1520-0380802	20.81	17.98	15.86	22554181+6204440	13.679	12.472	12.028	
J225542.0+621549.....	343.9252	62.2637	3.9	...	1.34	
J225542.9+621549.....	343.9291	62.2636	5.9	1.17	...	1522-0423549	15.48	13.54	13.03	
J225543.4+615618.....	343.9306	61.9384	6.7	...	2.48	1519-0362182	...	19.33	17.83	22554333+6156178	14.731	13.333	12.72	
J225544.6+620927.....	343.9359	62.1577	4.7	...	1.64	1521-0407199	...	18.82	16.85	22554471+6209283	14.474	13.322	12.914	
J225546.7+615739.....	343.9446	61.9610	10.9	...	5.41	1519-0362187	17.04	13.22	11.13	22554652+6157398	8.612	7.51	7.047	
J225547.2+621541.....	343.9471	62.2616	6.7	...	2.51	1522-0423568	19.52	16.01	14.81	22554696+6215415	13.024	11.976	11.546	

TABLE 2—*Continued*

XMMPT Source	R.A. (deg)	Decl. (deg)	σ	Soft (counts ks ⁻¹)	Hard (counts ks ⁻¹)	USNO-B1.0	<i>B</i>	<i>R</i>	<i>I</i>	2MASS	<i>J</i>	<i>H</i>	<i>K_s</i>	Notes
J225549.2+620502.....	343.9552	62.0839	4.6	...	1.49	
J225551.3+621314.....	343.9642	62.2207	5.4	...	2.16	
J225552.5+615727.....	343.9687	61.9577	6.2	...	2.46	
J225552.5+621358.....	343.9900	62.2329	4.1	0.72	
J225557.8+621356.....	343.9914	62.2324	5.2	...	1.81	1522-0423616	18.71	15.61	14.44	22555804+6213578	12.994	12.03	11.523	
J225558.7+615219.....	343.9948	61.8722	5.5	1.36	
J225601.6+620316.....	344.0072	62.0546	46.5	6.67	67.07	1520-0380840	18.24	14.08	13.58	22560182+6203165	11.457	10.275	9.71	HL 8
J225604.3+620303.....	344.0184	62.0509	30.9	2.26	34.96	1520-0380855	18.77	15.95	13.63	22560450+6203030	12.424	11.117	10.517	HL 9
J225604.7+620207.....	344.0200	62.0353	4.8	1.44	HH 168 X2
J225606.7+620433.....	344.0280	62.0759	10.2	...	6.58	1520-0380866	18.60	14.30	...	22560687+6204336	11.666	10.361	9.352	
J225607.1+620159.....	344.0296	62.0332	7.0	2.26	HH 168 X1
J225607.1+620230.....	344.0302	62.0418	9.7	...	5.53	22560733+6202287	17.659	13.997	12.084	WGA
J225607.4+620330.....	344.0315	62.0584	4.1	...	1.71	1520-0380873	...	19.41	17.55	22560761+6203307	13.526	11.777	10.75	
J225607.6+615800.....	344.0321	61.9667	5.1	1.14	...	1519-0362207	15.99	14.19	13.51	22560783+6158014	12.541	12.016	11.889	
J225608.4+621354.....	344.0355	62.2319	6.6	...	2.28	
J225608.6+615340.....	344.0362	61.8947	4.5	...	1.56	
J225609.3+615813.....	344.0386	61.9705	4.2	...	1.46	
J225611.5+620213.....	344.0475	62.0370	5.1	...	1.89	22561127+6202111	14.623	12.836	11.871	
J225612.4+621548.....	344.0518	62.2636	4.9	...	1.34	
J225612.7+620240.....	344.0535	62.0445	4.6	...	1.94	
J225613.2+620059.....	344.0547	62.0164	15.6	...	11.24	22561309+6200588	17.404	15.602	13.181	
J225613.4+620149.....	344.0556	62.0305	20.0	...	15.88	22561333+6201494	16.723	13.743	12.149	
J225613.6+615836.....	344.0568	61.9769	4.1	...	1.44	22561355+6158359	15.45	13.937	13.377	
J225614.6+620125.....	344.0606	62.0237	6.3	...	3.10	
J225615.1+620454.....	344.0632	62.0819	9.0	...	5.11	1520-0380894	...	18.80	16.67	22561539+6204545	13.844	12.382	11.814	
J225616.7+620033.....	344.0699	62.0094	6.9	...	3.10	22561679+6200323	17.642	14.759	13.146	
J225617.2+621021.....	344.0716	62.1726	4.6	...	1.59	1521-0407266	20.68	17.91	16.54	22561718+6210207	14.192	13.122	12.686	
J225617.2+615851.....	344.0724	61.9810	4.3	0.84	
J225618.4+620147.....	344.0766	62.0299	18.2	...	15.33	HWX
J225619.4+620223.....	344.0807	62.0397	4.8	...	2.26	
J225620.4+620221.....	344.0853	62.0392	5.4	1.34	...	1520-0380898	20.54	18.36	16.45	22562025+6202196	14.728	14.141	12.04	HL 28
J225621.1+620311.....	344.0877	62.0533	5.1	...	2.03	
J225622.0+620204.....	344.0919	62.0346	10.2	...	7.57	
J225625.9+615748.....	344.1076	61.9635	23.7	...	20.02	22562587+6157479	15.841	13.957	12.921	
J225626.6+615704.....	344.1112	61.9513	4.9	...	2.08	22562636+6157046	15.413	13.871	13.191	
J225628.5+620033.....	344.1187	62.0092	6.1	...	2.70	1520-0380902	...	19.43	18.01	22562823+6200331	14.71	13.274	12.62	
J225630.9+620002.....	344.1295	62.0008	16.8	...	10.82	1520-0380907	20.12	19.40	17.57	22563100+6200019	14.372	12.991	12.417	
J225631.2+621112.....	344.1301	62.1868	5.0	...	1.74	

TABLE 2—Continued

XMMPT Source	R.A. (deg)	Decl. (deg)	σ	Soft (counts ks ⁻¹)	Hard (counts ks ⁻¹)	USNO-B1.0	<i>B</i>	<i>R</i>	<i>I</i>	2MASS	<i>J</i>	<i>H</i>	<i>K_s</i>	Notes
J225631.4+615702.....	344.1312	61.9507	5.4	...	2.01	1519-0362229	...	18.58	16.57	22563141+6157013	13.945	12.84	12.385	
J225631.4+620128.....	344.1314	62.0246	7.3	...	3.62	1520-0380909	20.31	16.93	14.51	22563173+6201274	12.256	11.067	10.576	
J225637.6+615919.....	344.1570	61.9887	3.8	0.57	
J225640.5+620237.....	344.1686	62.0437	4.9	...	1.81	1520-0380925	20.81	18.13	16.38	22564070+6202374	13.847	12.717	12.296	
J225640.5+620104.....	344.1689	62.0179	18.4	...	12.80	1520-0380924	19.77	15.99	13.77	22564067+6201036	12.022	10.721	9.943	
J225640.5+620107.....	344.1691	62.0188	5.3	1.32	
J225641.5+620035.....	344.1727	62.0098	5.3	...	2.08	22564161+6200338	14.647	12.936	11.985	
J225642.0+620135.....	344.1746	62.0265	10.0	...	5.24	1520-0380926	20.74	17.54	15.67	22564195+6201347	13.02	11.737	11.247	
J225643.4+620730.....	344.1814	62.1250	15.6	4.54	5.24	1521-0407351	11.70	10.21	9.70	22564360+6207295	7.921	7.342	7.161	
J225643.9+615824.....	344.1827	61.9734	5.8	...	2.46	1519-0362241	20.73	17.43	15.68	22564375+6158225	13.319	12.207	11.765	
J225644.6+620326.....	344.1857	62.0573	7.2	...	3.37	1520-0380931	20.49	17.62	15.66	22564456+6203251	13.362	12.23	11.858	
J225644.8+615801.....	344.1874	61.9671	14.3	...	8.51	
J225645.1+615427.....	344.1876	61.9077	4.5	...	1.34	1519-0362244	...	19.56	18.09	22564503+6154271	14.71	13.239	12.736	
J225645.1+620657.....	344.1880	62.1159	6.2	...	2.63	
J225645.8+615208.....	344.1906	61.8689	6.5	...	2.73	1518-0358852	...	18.60	16.44	22564569+6152086	13.795	12.571	12.126	
J225646.0+615857.....	344.1923	61.9825	7.4	1.29	...	1519-0362245	19.39	17.04	15.72	22564618+6158577	14.246	13.578	13.397	
J225650.3+620944.....	344.2100	62.1622	7.2	...	3.05	
J225700.2+620441.....	344.2507	62.0781	4.9	...	1.84	22570014+6204391	15.424	13.869	13.306	
J225700.7+621104.....	344.2533	62.1846	7.1	...	2.83	1521-0407391	...	20.05	17.71	22570090+6211041	15.251	13.974	13.501	
J225704.7+615523.....	344.2701	61.9231	4.7	...	1.76	22570501+6155248	13.802	12.288	11.466	
J225708.4+620245.....	344.2848	62.0460	6.1	...	2.58	
J225728.8+620244.....	344.3699	62.0457	5.8	...	2.16	1520-0381002	20.22	17.57	14.82	22572881+6202438	13.621	12.495	12.077	
J225729.0+615704.....	344.3707	61.9513	10.0	...	4.71	1519-0362326	20.27	17.05	14.74	22572891+6157039	13.105	12.003	11.571	
J225737.1+615756.....	344.4046	61.9658	8.4	...	3.97	1519-0362346	17.76	15.48	14.32	22573680+6157560	13.099	11.789	10.856	

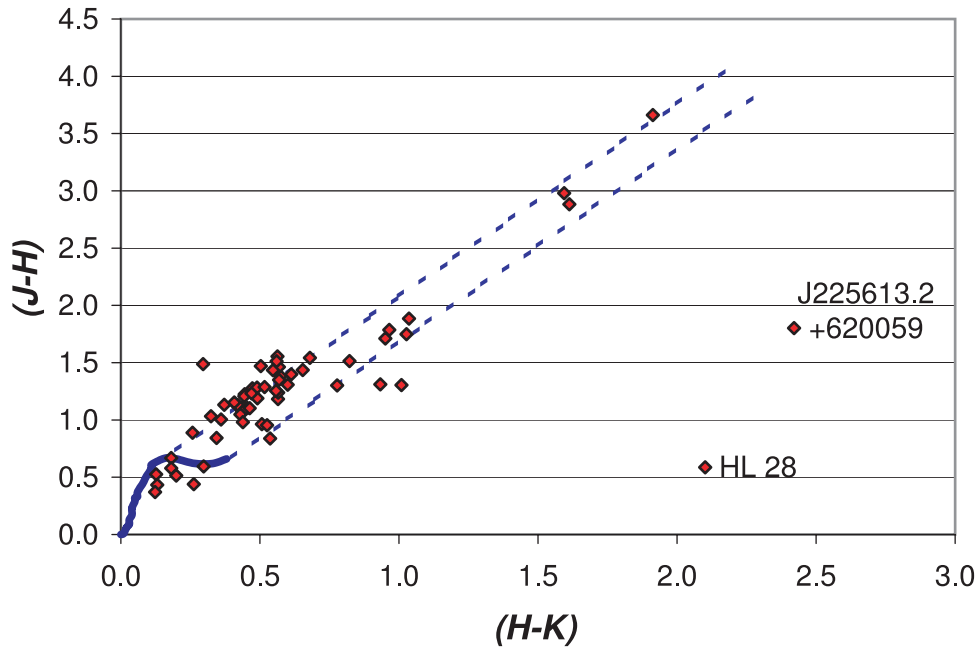


FIG. 2.—Color-color JHK diagram for the infrared counterparts to the X-ray sources in the Cep A field. The solid line is the main sequence, and the dashed lines are the reddening lines.

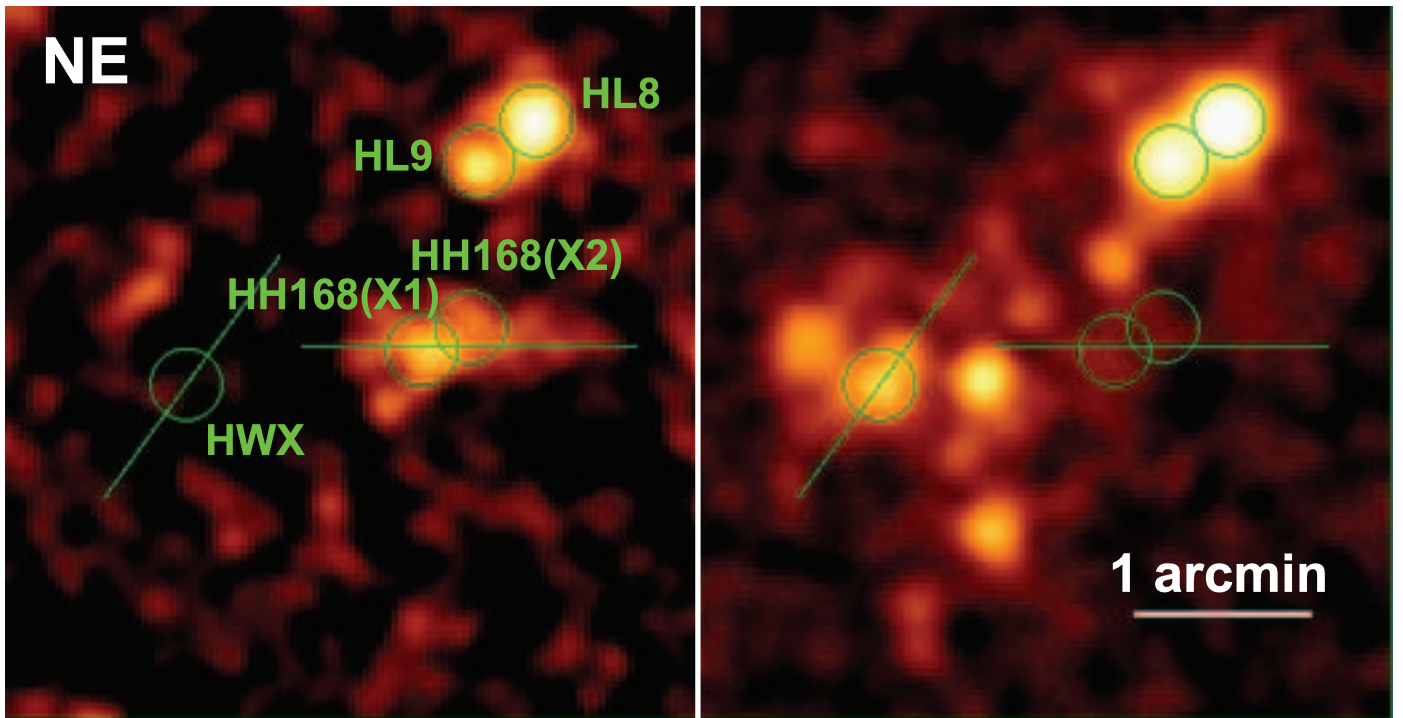


FIG. 3.—*XMM-Newton* MOS maps of the HH 168 and HWX regions. The data were rebinned into $2''4 \times 2''4$ pixels and smoothed with a $4''8 \sigma$ Gaussian. On the left is the 0.2–1 keV image. On the right is the 1–10 keV image. The lines through the source show the axes on which the linear profiles shown in Fig. 5 were taken.

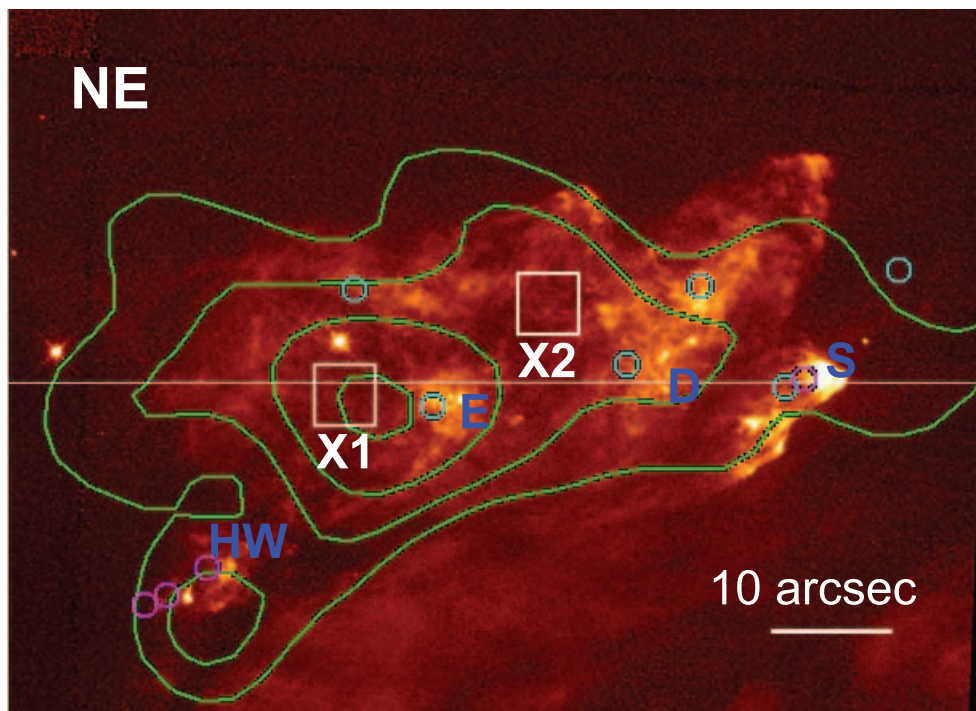


FIG. 4.—Plot of the 0.2–1.0 keV *XMM-Newton* X-ray contours (0.47, 0.64, and 0.87 counts arcsec⁻²) superposed on the *HST* WFPC2 image of Cep A taken with the H α filter (Hartigan et al. 2000). The circles are compact radio sources: blue circles are from Hughes & Moriarty-Schieven (1990), and purple circles are from Garay et al. (1996). The boxes show the locations of the X-ray sources X1 and X2.

or a power law. The thermal model with a temperature of $T = 5.8^{+3.5}_{-2.3} \times 10^6$ K and interstellar absorption of $N_{\text{H}} = (4 \pm 4) \times 10^{21} \text{ cm}^{-2}$ yields the best fit (see Table 3).

2.3. HWX

A hard-spectrum and non-pointlike X-ray source, XMMPT J225618.4+620147 (hereafter HWX), is located near the center of the radio activity in Cep A East. Figure 3 (*right*) shows the smoothed MOS X-ray image in the 1–10 keV band and the detected sources. Note that the reverse of the HH 168 situation holds: HWX is a predominantly hard X-ray source, undetectable in the softer X-ray image. Figure 5 (*right*) shows a comparison of the HWX linear spatial profile along the line shown

in Figure 3 with that of RX J171012.3–28075, a putative point source. Again, the HWX profile is extended and/or contains multiple sources. Figure 6 shows *XMM-Newton* MOS contours superposed on the 2MASS K_s image containing HWX. We also show the compact radio sources (*small circles*). The HWX emission appears to run in a ridge, approximately southeast to northwest, that encompasses some of the radio sources. The sources HW 3d and HW 9 are nearest to the center of the X-ray emission, with separations of $\sim 1''8$.

The HWX X-ray spectrum is unusually hard, in contrast with that of HH 168 (Fig. 7). It fits a thermal spectrum with $T = 1.2^{+1.2}_{-0.5} \times 10^8$ K with $N_{\text{H}} = 8^{+3}_{-2} \times 10^{22} \text{ cm}^{-2}$, which corresponds to 36^{+14}_{-9} visual magnitudes of absorption. The spectrum fits

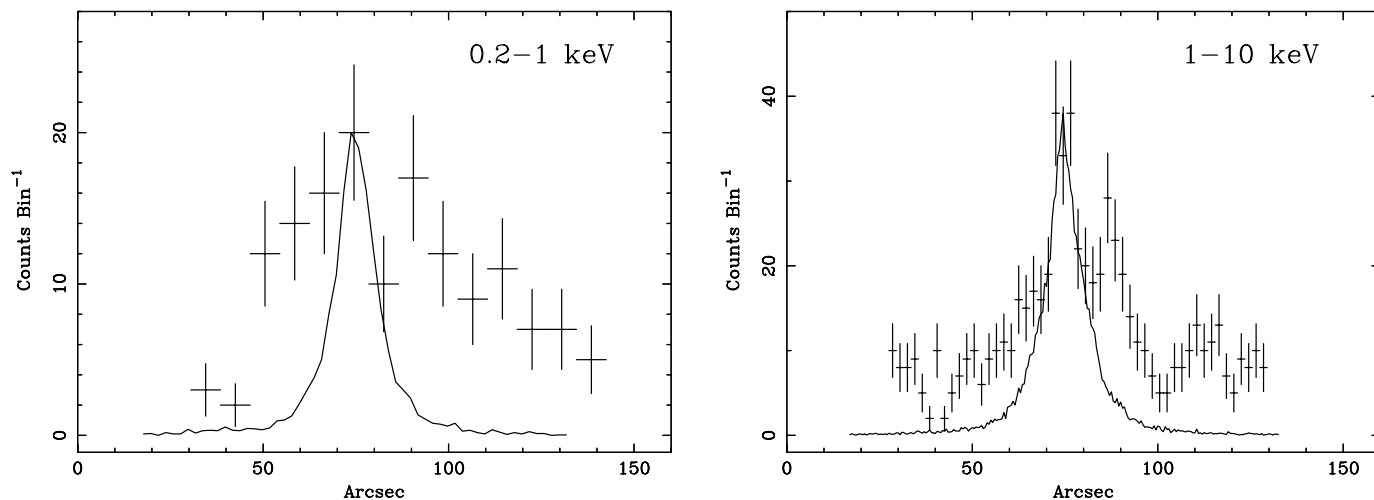


FIG. 5.—Comparison of the X-ray spatial radial profiles between (*left*) HH 168 in the soft band and the putative point source RX J171012.3–28075 (Y. Maeda 2004, private communication) and (*right*) HWX in the hard band and the same point source.

TABLE 3
SPECTRAL PARAMETERS OF SELECTED X-RAY SOURCES IN THE Cep A FIELD

XMMPT Source	Net Counts	kT (keV)	N_{H} (10^{22} cm^{-2})	I (0.2–2 keV) ($10^{-15} \text{ ergs cm}^{-2} \text{ s}^{-1}$)	I (2–10 keV) ($10^{-15} \text{ ergs cm}^{-2} \text{ s}^{-1}$)
HH 168 composite.....	150	$0.5^{+0.3}_{-0.2}$	0.4 ± 0.4	3.5	...
HWX.....	300	10^{+10}_{-4}	8^{+3}_{-2}	0.2	131
J225454.9+615936.....	204	$0.6^{+0.1}_{-0.4}$	0.5 ± 0.2	18	1.6
J225643.4+620730.....	160	$0.4^{+0.3}_{-0.2}$	0.8 ± 0.4	9.2	0.36
HL 8.....	934	0.3 and 2.2	1.8	36	93
HL 9.....	385	$4.9^{+10}_{-2.6}$	$0.5^{+0.5}_{-0.3}$	20	68

equally well to a power-law continuum with $\alpha = 0.3$. The X-ray light curve of HWX was measured within a radius of $12''$ in the 1–10 keV band. There is an indication of variability at the 95% confidence level.

2.4. Other Sources

XMMPT J225454.9+615936 is a source that was probably detected with the *ROSAT* HRI (Zombeck et al. 1990) on 1996 December 17. Since the HRI observation was $15'$ off-axis, its point-spread function of several arcseconds allows for the identification of this isolated X-ray source despite its $3''$ separation from the *XMM-Newton* position. The colors resemble those of an M0 V star (see Table 3). If it is an M0 V star, its distance is ~ 130 pc, making it a foreground object. Its *XMM-Newton* spectrum is relatively soft, with $T = 7.0^{+1.2}_{-4.6} \times 10^6$ K. The 0.2–2.0 keV X-ray intensity was $\sim 1 \times 10^{-13} \text{ ergs cm}^{-2} \text{ s}^{-1}$ from HRI and $\sim 2 \times 10^{-14} \text{ ergs cm}^{-2} \text{ s}^{-1}$ from *XMM-Newton*, with evidence of variability by a factor of ~ 5 . There is no evidence for variability or periodicity, however, in the current data alone. If XMMPT J225454.9+615936 is at 130 pc, its X-ray luminosity is $0.4\text{--}2 \times 10^{29} \text{ ergs s}^{-1}$, on the high end of the luminosity function for this spectral type (Hünsch et al. 1999).

The two brightest *XMM-Newton* sources are associated with the optical stars HL 8 (=J225601.6+620316) and HL 9 (=J225604.3+620303). Hartigan & Lada (1985) found these stars to be weak $H\alpha$ emitters and measured $(R, I) = (15.75, 13.98)$ and $(17.51, 15.49)$ for HL 8 and HL 9, respectively, which is 0.5–1.5 mag fainter than the USNO-B1.0 values (Table 2). On the basis of their M_J and $J - K$ values, these may be K–M stars. The single-component X-ray spectrum of HL 8 fits a power-law model far better than a thermal model (reduced χ^2 of 1.6 compared with 3.8). However, for a stellar spectrum there is no good physical interpretation for a power-law spectrum with a photon index of ~ 2.3 . There is no apparent variability or periodicity in the X-rays that might support a nonthermal origin. A two-component thermal model, however, also fits. Such a model has been used in the past to interpret PMS spectra (e.g., Feigelson et al. 2002). HL 9 fits a thermal spectrum and also appears to be a PMS star.

The *XMM-Newton* source with the brightest optical/NIR counterpart is XMMPT J225643.4+620730. It may also be a foreground object with a soft X-ray spectrum (Table 3), although its colors are reddened. Its X-ray luminosity is $\sim 6 \times 10^{29} \text{ ergs s}^{-1}$ at the distance of Cep A.

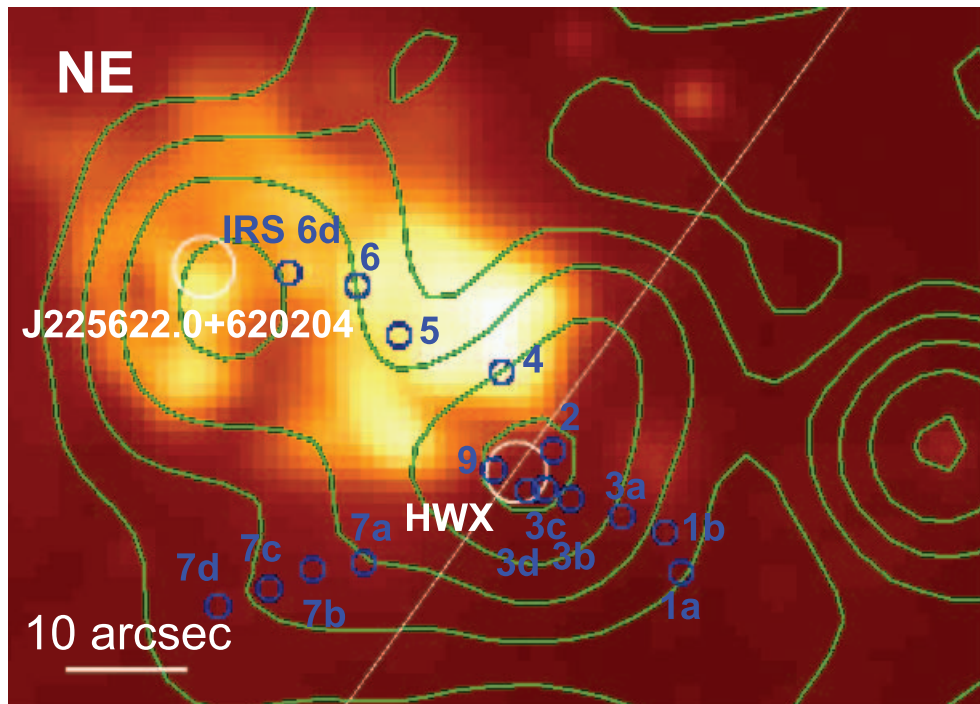


FIG. 6.—Plot of the 1–10 keV *XMM-Newton* MOS X-ray contours (0.24, 0.33, 0.46, and 0.64 counts arcsec $^{-2}$) of the Cep A East region superposed on the 2MASS K_s image. We also show the locations of the detected hard X-ray sources (large circles; $2''.5$ radius) and compact radio sources (small circles; Hughes & Wouterloot 1984; Hughes 1991; Goetz et al. 1998).

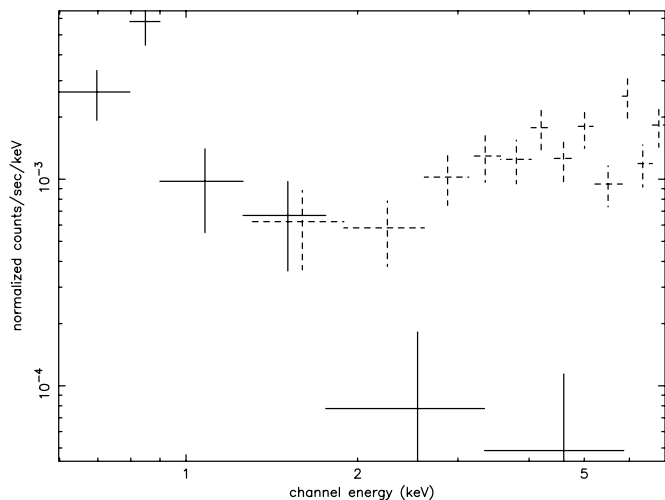


FIG. 7.—Comparison of the soft X-ray spectrum of HH 168 (solid symbols) with the hard X-ray spectrum of HWX (dashed symbols).

The two reddest sources are labeled in the *JHK* color-color diagram (Fig. 2). XMMPT J225620.4+620221 is a soft X-ray source, identified as HL 28 (Hartigan & Lada 1985), an unremarkably red star in the optical. XMMPT J225613.2+620059 is a hard X-ray and IR source with no optical counterpart.

3. DISCUSSION

3.1. X-Rays from HH 168

We conclude that HH 168 joins the growing list of HH objects that are soft X-ray sources, despite the challenging morphology discussed below. The HH objects that have been detected, HH 2H (Pravdo et al. 2001), HH 154 (Favata et al. 2002), and HH 80/81 (Pravdo et al. 2004), are the ones with the highest velocities and highest optical excitations and are associated with compact 6 cm radio emission sources. HH 168 qualifies with respect to velocity (Lenzen et al. 1984), excitation (Hartigan et al. 1986, 2000), and radio emission (Hughes & Moriarty-Schieven 1990).

The HH 168 X-ray emission appears to be extended, although the spatial resolution of *XMM-Newton* is not sufficient to resolve weak point sources $1''$ – $2''$ apart. The X-ray contours in Figure 4 show a good correlation between the extents of the X-ray and the $H\alpha$ emission. However, whereas in HH 80/81 there is a clear positional correlation between peaks of X-ray and $H\alpha$ intensity (Pravdo et al. 2004), the X-ray peaks in HH 168 are offset from those in $H\alpha$ by $\sim 8''$. Knot proper motions of $\sim 0''.03 \text{ yr}^{-1}$ (Lenzen 1988) cannot account for this, since the $H\alpha$ observations were made in 1998. Furthermore, HH 168 X-rays do not appear at the leading edges of the westerly moving knots, in contrast with the HH 2H emission (Pravdo et al. 2001). On the other hand, there is no reason to associate the X-rays with another source: for example, the star HL 14, about $5''$ north of the stronger X-ray peak.

The luminosity of the composite HH 168 X-ray emission is $1.1 \times 10^{29} \text{ ergs s}^{-1}$, assuming that the observed low-energy absorption is interstellar. This is the lowest of all the observed HH objects. If the X-rays arise in a shock with the measured X-ray temperature, then the inferred shock velocity is $v_s \sim (T/15)^{1/2} = 620_{-140}^{+170} \text{ km s}^{-1}$, larger than the optical knot line widths and only marginally consistent with the $\sim 475 \text{ km s}^{-1}$ line width measured by Hartigan et al. (1986) in the HW knot to the southeast edge of the X-ray emission contour. The temperature is higher than that measured in the other HH objects. Closest is the temperature of HH 154, $T \sim 4 \times 10^6 \text{ K}$ (Favata et al. 2002), modeled as originating in the inner portions of the outflow (Bally et al. 2003).

Figure 8 shows a plot of X-ray versus radio emission for the known X-ray HH objects. HH 168 in toto appears to be underluminous in X-rays relative to its radio emission (Garay et al. 1996). We also show the function $L_X \sim L_R^{1.4}$, the best fit for these data. The fit has a spectral index error of ± 0.5 and so is marginally consistent with a linear relationship or an index of 1.24, which Güdel (2002) shows is appropriate for L_X versus L_R of stars, wherein the energy arises from the magnetic fields. Applying the model of Raga et al. (2002) to HH 168, we find that the X-ray emission regions are nonradiative, with a pre-shock number density, $n_0 \sim 10 \text{ cm}^{-3}$, where we have divided

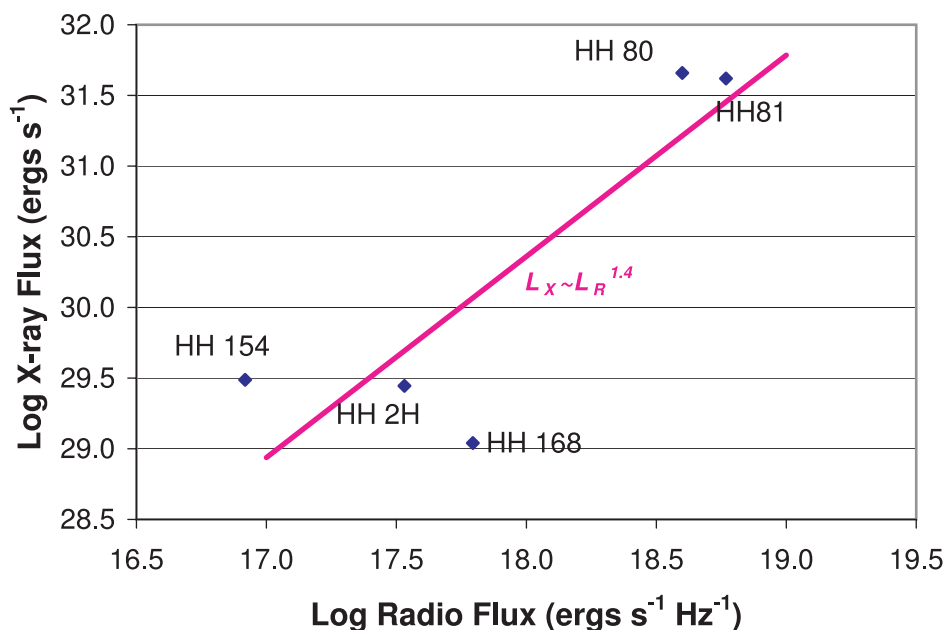


FIG. 8.—Relationship between X-ray and radio (6 cm) luminosity for the known X-ray-emitting HH objects. The solid line is a linear fit to these data.

the emission among ~ 2 hot spots, each with the volume of the HH 168 knot E.

Why are the HH 168 X-rays both underluminous and offset from the bright optical and radio regions? The answer may lie in the complex geometry of the region and the tangled locations of possible power sources. Ho et al. (1982) conclude that ambient density anisotropies in Cep A lead to outflows that are not well collimated. One can imagine holey Swiss cheese-like regions from whence the X-rays penetrate in varying amounts, leading to an extended, spatially varying flux profile. Since different density regions preferentially emit at radio, optical, and X-ray wavelengths, the randomization of the emitting and absorbing masses along the lines of sight could create the observed lack of correlation.

3.2. The Nature of HWX

Radio observations of Cep A East show many compact radio sources, some with quasilinear structure (Hughes & Wouterloot 1984) and some that are variable (e.g., Hughes 1991). Hughes (1988) identified these as PMS stars on the basis of their variability and association with masers. HWX is located at the radio “hub” identified by many observers as the location of the power source or sources of at least Cep A East. Figure 6 shows that there is an anticorrelation between the HWX X-rays (and most of the radio sources) and the nebular emission, suggesting that X-rays to the northeast are absorbed, i.e., in the direction of HW 4–HW 6. The hard, absorbed HWX spectrum (Fig. 7) is in keeping with the idea that X-rays emerge from the edge of a highly absorbed region. The hard spectrum also distinguishes HWX, despite its possible extent, from HH 168 and other HH sources that are believed to originate from diffuse jets. The “blank field” X-ray source XMMPT J225622.0+620204 emerges from the IR nebula at the end of the string of radio sources extending to the northeast, $\sim 7''$ from IRS 6d (Goetz et al. 1998).

The peak of the complex HWX emission (Figs. 3 and 5, *right*) is consistent with a single point source, with the remaining emission due to either additional point sources and/or diffuse emission. Both HW 3d and HW 9 lie within our $2''5$ criterion for an association. Torrelles et al. (1998) resolved HW 3d into four radio continuum sources. Of these, HW 3di, HW 3dii, and HW 3div are coincident with HWX. HW 3dii is a dominant source associated with H₂O and OH masers (Migenes et al. 1992) and is believed by Torrelles et al. (1998) to be the second youngest in the Cep A region. The HW 3dii coincidence with masers and its positive spectral index (Garay et al. 1996) suggest that it contains a young stellar object (YSO) with our detected hard X-ray emission. HW 9 is variable, appearing and disappearing over ~ 100 days (Hughes 1991). Hughes (1991) concluded that its radio emission was consistent with gyrosynchrotron emission from a region of ~ 1 AU with a temperature of $\sim 10^8$ K and a magnetic field of ~ 200 G. He interpreted the high electron temperature as a result of magnetic reconnection. However, we note that the thermal emission from such a region is only a few percent of the HWX emission. Other nearby radio sources, including HW 2, also lie in an area of X-ray emission offset from the main peak (Fig. 6). The reason that the highly energetic HW 2, often fingered as the Cep A power source, is not more prominent in X-rays may be because it is even more highly absorbed than HWX. Torrelles et al. (1993) estimate a molecular hydrogen column density of $\sim 10^{24}$ cm⁻², or $N_{\text{H}} \sim 2 \times 10^{24}$ cm⁻², ~ 20 times higher than the HWX measurement.

The HWX X-ray spectrum is highly absorbed, with an N_{H} corresponding to $A_V \sim 36$ mag (Gorenstein 1975), typical of

the high absorptions invoked to hide the stellar (e.g., Lenzen et al. 1984) or protostellar sources (e.g., Imanishi et al. 2001; Tsuboi et al. 2001). The inferred unabsorbed X-ray luminosity, $\sim 1.6 \times 10^{31}$ ergs s⁻¹, is larger than the typical values for low-mass protostars in quiescent phases, 1×10^{29} – 4×10^{30} ergs s⁻¹ for Class I candidates (Imanishi et al. 2001) and $\sim 10^{30}$ ergs s⁻¹ for Class 0 candidates (Tsuboi et al. 2001), although it is smaller than that of the extreme protostars SSV 63 E+W in quiescence, $\sim 1 \times 10^{32}$ ergs s⁻¹ in total (Ozawa et al. 1999). Flaring low-mass protostars can reach the HWX level with X-ray luminosities of 10^{30} – 10^{32} ergs s⁻¹ (e.g., Imanishi et al. 2001). On the other hand, the luminosity is also on the high end for high-mass embedded YSOs (e.g., Kohno et al. 2002). The extremely high temperature of HWX (100 MK) is only seen in large flares in low-mass stars (e.g., Tsuboi et al. 1998; Imanishi et al. 2001) or the time-varying emission from plasma from the high-mass YSO IRS 2 in Monoceros (Kohno et al. 2002). All these are indicators that HWX is in a high state of X-ray activity, whether it is low mass or high mass.

Another noteworthy discovery is a hard X-ray ridge along the chain of HW 7a–7d (Figs. 3 and 6). The HW 7 chain is interpreted from the radio spectrum as material shocked by a jet. HW 7d, with a peculiar velocity of 300 km s⁻¹, appears to be at the head of the jet (Hughes 1993). Hughes (1993) suggests that HW 9 could be the power source, while Garay et al. (1996) choose HW 3d. Again, these are the two sources with the closest association with HWX. This chain is also along the “high-velocity” outflow seen from near HW 2 to HW 7 in infrared line emission (Goetz et al. 1998). This X-ray ridge cannot be seen in the soft-band image (Fig. 3), indicating that it arises from a hard and absorbed X-ray spectrum like HWX. If the ridge is as hard as HWX, an origin from a high-velocity shock would require jets moving at ~ 2000 km s⁻¹, a much higher velocity than that of the observed motion of HW 7d. Hughes (2001) speculates that if HW 7d originated in HW 3d (or its neighbors), then its age is ~ 340 yr. If HWX is associated with this power source, then we may be viewing a Class 0 protostar relatively early in its $\sim 10^4$ yr lifetime (Feigelson & Montmerle 1999).

A final morphological point to note is that the terminus of the Goetz et al. (1998) “extreme high velocity” outflow is in the nebula proper, near IRS 6d and XMMPT J225622.0+620204 (Fig. 6). This source has fewer net counts than HWX, and its spectral parameters, while consistent with those of HWX, are not meaningfully constrained. Its unabsorbed luminosity is $\sim 7 \times 10^{30}$ ergs s⁻¹.

4. CONCLUSIONS

We performed the first high-sensitivity and moderate spatial resolution X-ray observation of Cep A and began to untangle the X-ray morphologies of both Cep A East and West. HH 168 is detected in X-rays and has some, but not all, of the characteristics of previously discovered X-ray HH objects. HWX is located in the region identified at other wavelengths as the location of the Cep A power sources, but the X-ray evidence is ambiguous as to whether we are seeing the sources, the outflows, or perhaps a combination of both. A more secure indication of short-term HWX variability would favor its stellar or protostellar origin. If HWX were composed of several protostars, higher resolution and higher sensitivity measurements would provide valuable information regarding their X-ray spectra and luminosities. HWX is harder than the HH jets seen in X-rays. However, if HWX were a jet, it might lie closer to its power sources and thus be more energetic, with a resulting higher temperature.

The research described in this paper was performed in part by the Jet Propulsion Laboratory, California Institute of Technology, under contract with the National Aeronautics and Space Administration (NASA). Y. T. acknowledges partial support from a Grant-in-Aid for Scientific Research of the Ministry of Education, Culture, Sports, Science, and Technology (15740120) and from a Chuo University Grant for Special Research. Y. T. also thanks the Saneyoshi Scholarship Foundation for their financial support. We thank Y. Maeda for useful discussions and for providing the RX J171012.3–28075 data prior to publication. We thank S. Snowden, M. Arida, and HEASARC for extensive help with *XMM-Newton* data analysis. P. Hartigan graciously provided the processed *HST* image for our use. We also thank the *XMM-Newton* User Support.

This research has made use of the NASA/IPAC Infrared Science Archive, which is operated by the Jet Propulsion Laboratory, California Institute of Technology, under contract with NASA. This research has made use of the SIMBAD database, operated at CDS, Strasbourg, France. Some of the data presented in this paper were obtained from the Multimission Archive at the Space Telescope Science Institute. The Association of Universities for Research in Astronomy, Inc., operates the Space Telescope Science Institute under NASA contract NAS5-26555. This publication makes use of data products from the Two Micron All Sky Survey, which is a joint project of the University of Massachusetts and the Infrared Processing and Analysis Center/California Institute of Technology, funded by NASA and the National Science Foundation.

REFERENCES

- Bally, J., Feigelson, E., & Reipurth, B. 2003, *ApJ*, 584, 843
 Beichman, C. A., Becklin, E. E., & Wynn-Williams, C. G. 1979, *ApJ*, 232, L47
 Blitz, L., & Lada, C. J. 1979, *ApJ*, 227, 152
 Casement, L. S., & McLean, I. S. 1996, *ApJ*, 462, 797
 Favata, F., Fridlund, C. V. M., Micela, G., Sciortino, S., & Kaas, A. A. 2002, *A&A*, 386, 204
 Feigelson, E. D., Broos, P., Gaffney, J. A., III, Garmire, G., Hillenbrand, L. A., Pravdo, S. H., Townsley, L., & Tsuboi, Y. 2002, *ApJ*, 574, 258
 Feigelson, E. D., & Montmerle, T. 1999, *ARA&A*, 37, 363
 Garay, G., Ramírez, S., Rodríguez, L. F., Curiel, S., & Torrelles, J. M. 1996, *ApJ*, 459, 193
 Goetz, J. A., et al. 1998, *ApJ*, 504, 359
 Gorenstein, P. 1975, *ApJ*, 198, 95
 Güdel, M. 2002, *ARA&A*, 40, 217
 Gyulbudaghian, A. L., Glushkov, Y. I., & Denisjuk, E. K. 1978, *ApJ*, 224, L137
 Hartigan, P., & Lada, C. J. 1985, *ApJS*, 59, 383
 Hartigan, P., Lada, C. J., Stocke, J., & Tapia, S. 1986, *AJ*, 92, 1155
 Hartigan, P., Morse, J., & Bally, J. 2000, *AJ*, 120, 1436
 Ho, P. T. P., Moran, J. M., & Rodríguez, L. F. 1982, *ApJ*, 262, 619
 Hughes, V. A. 1988, *ApJ*, 333, 788
 ———. 1991, *ApJ*, 383, 280
 ———. 1993, *AJ*, 105, 331
 ———. 2001, *ApJ*, 563, 919
 Hughes, V. A., & Moriarty-Schieven, G. 1990, *ApJ*, 360, 215
 Hughes, V. A., & Wouterloot, J. G. A. 1982, *A&A*, 106, 171
 ———. 1984, *ApJ*, 276, 204
 Hünsch, M., Schmitt, J. H. M. M., Sterzik, M. F., & Voges, W. 1999, *A&AS*, 135, 319
 Imanishi, K., Koyama, K., & Tsuboi, Y. 2001, *ApJ*, 557, 747
 Johnson, H. L. 1957, *ApJ*, 126, 121
 Kohno, M., Koyama, K., & Hamaguchi, K. 2002, *ApJ*, 567, 423
 Lenzen, R. 1988, *A&A*, 190, 269
 Lenzen, R., Hodapp, K.-W., & Solf, J. 1984, *A&A*, 137, 202
 Migenes, V., Cohen, R. J., & Brebner, G. C. 1992, *MNRAS*, 254, 501
 Monet, D. G., et al. 2003, *AJ*, 125, 984
 Ozawa, H., Nagase, F., Ueda, Y., Dotani, T., & Ishida, M. 1999, *ApJ*, 523, L81
 Pravdo, S. H., Feigelson, E. D., Garmire, G., Maeda, Y., Tsuboi, Y., & Bally, J. 2001, *Nature*, 413, 708
 Pravdo, S. H., Tsuboi, Y., & Maeda, Y. 2004, *ApJ*, 605, 259
 Raga, A. C., Noriega-Crespo, A., & Velázquez, P. F. 2002, *ApJ*, 576, L149
 Rodríguez, L. F., Garay, G., Curiel, S., Ramírez, S., Torrelles, J. M., Gómez, Y., & Velázquez, A. 1994, *ApJ*, 430, L65
 Rodríguez, L. F., Ho, P. T. P., & Moran, J. M. 1980, *ApJ*, 240, L149
 Sargent, A. I. 1977, *ApJ*, 218, 736
 Torrelles, J. M., Gómez, J. F., Garay, G., Rodríguez, L. F., Curiel, S., Cohen, R. J., & Ho, P. T. P. 1998, *ApJ*, 509, 262
 Torrelles, J. M., Ho, P. T. P., Rodríguez, L. F., & Cantó, J. 1985, *ApJ*, 288, 595
 Torrelles, J. M., Rodríguez, L. F., Cantó, J., & Ho, P. T. P. 1993, *ApJ*, 404, L75
 Tsuboi, Y., Koyama, K., Hamaguchi, K., Tatematsu, K., Sekimoto, Y., Bally, J., & Reipurth, B. 2001, *ApJ*, 554, 734
 Tsuboi, Y., Koyama, K., Murakami, H., Hayashi, M., Skinner, S., & Ueno, S. 1998, *ApJ*, 503, 894
 Zombeck, M. V., Conroy, M., Hamden, F. R., Roy, A., Bräuninger, H., Burkert, W., Hasinger, G., & Predehl, P. 1990, *Proc. SPIE*, 1344, 267